Water distribution in the lower mantle: Implications for hydrolytic weakening

Joshua M.R. Muir *, John P. Brodholt

Department of Earth Sciences, University College London, Gower Street, London, WC1E 6BT, UK

A B S T R A C T

The presence of water in lower mantle minerals is thought to have substantial effects on the rheological properties of the Earth's lower mantle in what is generally known as "hydrolytic weakening". This weakening will have profound effects on global convection, but hydrolytic weakening in lower mantle minerals has not been observed experimentally and thus the effect of water on global dynamics remains speculative. In order to constrain the likelihood of hydrolytic weakening being important in the lower mantle, we use first principles methods to calculate the partitioning of water (strictly protons) between mineral phases of the lower mantle under lower mantle conditions. We show that throughout the lower mantle water is primarily found either in the minor Ca-perovskite phase or in bridgmanite as an Al^{3+}–H^+ pair. Ferropericlase remains dry. However, neither of these methods of water absorption creates additional vacancies in bridgmanite and thus the effect of hydrolytic weakening is likely to be small. We find that water creates significant number of vacancies in bridgmanite only at the deepest part of the lower mantle and only for very high water contents (>1000 ppm). We conclude that water is thus likely to have only a limited effect on the rheological properties of the lower mantle.

1. Introduction

A growing number of studies are finding that incorporating a water dependent rheology into global mantle convection models has a strong effect on global dynamics. For instance the feedback between water recycling and rheology can control mantle cooling history, the efficiency and timescale of water recycling, the initiation of plate tectonics, continental growth, and the formation of dense chemical anomalies (Crowley et al., 2011; Korenaga, 2011; Sandu et al., 2011; Nakagawa et al., 2015; Honing and Spohn, 2016). These results are based on the assumption that water has a strong effect on the rheological properties of mineral and rocks (hydrolytic weakening) and that this occurs throughout the convecting mantle. However, while there is an abundance of experimental evidence showing that upper mantle minerals deformed under hydrous conditions are significantly weaker than when dry (e.g. Griggs and Blacic, 1965; Karato et al., 1986; Mei and Kohlstedt, 2000a, 2000b; Karato and Jung, 2003; Faul et al., 2016), there is no such experimental evidence for lower mantle minerals.

Although the exact mechanism for hydrolytic weakening in upper mantle minerals is still in debate (Fei et al., 2013), the most likely reason is that water increases the number of vacancies available for diffusion (Kohlstedt, 2006; Faul et al., 2016). This in turn lowers the viscosity either through diffusion creep or via diffusion-controlled dislocation climb. In order to evaluate the likelihood that hydrolytic weakening also occurs in lower mantle minerals, we need to know, therefore, how water partitions between the different lower mantle phases and how water affects the concentration of deformation-controlling defects. To approach this problem we have calculated the energetics of water partitioning between various lower mantle mineral sites using Density Functional Theory (DFT) which allows us to simulate the high pressure and high temperature conditions of the lower mantle that are hard to replicate experimentally.

2. Methods

Our overall method is to use *ab initio* molecular dynamics (MD) simulations to calculate the free energy of dry and hydrous ferropericlase, aluminous bridgmanite, calcium perovskite and δ-AlOOH and $MgSiO_4H_2$ at 25 and 125 GPa. Free energies were obtained as linear functions of temperature and water content, and polynomial functions of temperature. A mixture of phases representing the lower mantle was constructed, and with a fixed water content the concentrations and site locations of water were determined by solving partitioning reactions that transfer the water between various mineral sites and phases.
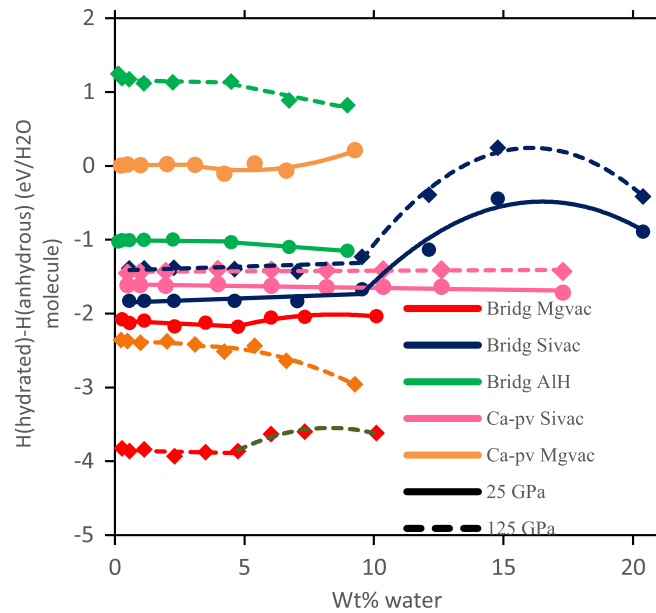
Fig. 1. Variation of the hydration enthalpy (defined as the enthalpy difference between a hydrated structure and an anhydrous structure) with increasing water concentration for different adsorption sites at 25 and 125 GPa. Lines represent 2 fits, one up to 4 wt% where enthalpy changes are essentially linear with concentration and one above 4 wt% where more complex behaviour is observed.
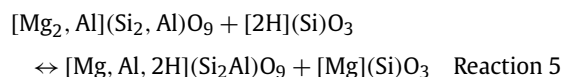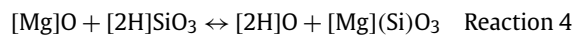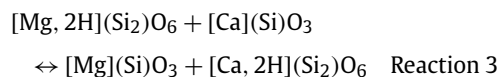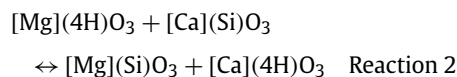
All simulations were carried out with the DFT code VASP (Kresse and Furthmuller, 1996) using the projector-augmented-wave (PAW) method (Kresse and Joubert, 1999) and the PBE formulation of GGA (Perdew et al., 2008) with the standard PAW-PBE VASP pseudopotentials used (Mg_pv, Ca_sv, H, Si and O). As our cells had unpaired H atoms we tested long range dispersion using the DFT-D3 method of Grimme (Grimme et al., 2010) and the DFT-TS method of Tkatchenko–Scheffler (Tkatchenko and Scheffler, 2009) at static conditions and found no difference in optimised geometry or enthalpy than with non-D methods. Static calculations (to determine static enthalpy differences of reactions) were run with an energy cutoff of 850 eV, $(6 \times 6 \times 6)$ k points and self-consistent runs that were relaxed to within 10^{-6} eV. MD simulations (to determine thermal effects on energy differences) were run to obtain properties at high T using an NVT ensemble with the Nosé thermostat (Nose, 1984) and with Nosé frequencies of ∼20 THz. MD calculations were run at the gamma point with a cutoff of 600 eV, relaxation to within 10^{-4} eV and were run for at least 30 ps though all measured properties were fully relaxed by 12 ps. For Mg atoms the semicore 2p states were treated as valence and for Ca the semicore 3s and 3p states were treated as valence. All static and molecular dynamics runs were spin-polarised.

Water is treated as a replacement of protons for cations in each mineral structure, with each proton forming an OH pair. Water was simulated in Ca/Mg/Si vacancies in bridgmanite, ferropericlase, calcium perovskite and in Al–H pairs in bridgmanite by removing the cation and replacing it with 2 (Ca/Mg) or 4 (Si) H atoms and in δ-AlOOH and $MgSiO_4H_2$ phases where the H is bound in the structure. Both tetragonal and cubic $CaSiO_3$ were simulated, with the lowest energy phase (which depends upon P, T and water concentration) used. Conditions at the top (25 GPa 1000/2000 K) and near the bottom of the lower mantle (125 GPa 1000/2000/3000 K) were simulated. Below 125 GPa the post-perovskite phase may become stable, but that has not been considered here. Static cutoffs were 850 eV with $(6 \times 6 \times 6)$ k-points, and dynamics cutoffs were 600 eV with the gamma point. Unit cell sizes were 80 atoms for the pv phases and 64 for fp and H-phases. δ-AlOOH and $MgSiO_4H_2$ crystal structures were built with a space group of P21nm and

a Pnnm respectively. Energies were determined with 1 Si or Mg (Ca) vacancy filled with 2 H (for Mg vacancies) or 4 H (for Si vacancies). This is a concentration of 1.1 (1.0) wt% water in the Mg (Ca) vacancy and 2.3 (2.0 in Ca-pv) in the Si vacancy. To simulate Al-pv we replaced an Mg-Si pair in the 80 atom unit cell of pv with an Al–Al pair ($AlMg_{15}AlSi_{15}O_{48}$) which equates to an Al_2O_3 concentration of wt% of 6.3. The enthalpy of Al substitution was found to be linear with Al concentration (as outlined in the supplementary materials) and so the energy was then scaled from 6.3 wt% to 5 wt% Al_2O_3. To simulate the introduction of Al–H, either 1 or 2 Si atoms were replaced by an Al–H pair in the 80 atom unit cell (no difference was found between these systems).

To test the effect of water concentration we removed between 1 and 8 Mg/Ca/Si from the 80 atom unit cell and replaced them with H atoms. Due to computational constraints, this was only done at 0 K. To test lower water concentrations, we placed one hydrous vacancy in a larger 160 and 320 atom unit cell. This covers a concentration of 0.3 to 10% wt% water in Mg/Ca vacancies and 0.6 to 20 wt% in Si vacancies. For $MgSi_{1-x}(AlH)_xO_3$ we tested all values of x in an 80 atom unit cell and with 1 AlH pair in a 160 and 320 atom unit cell, which gives a water concentration of 0.1 to 9 wt%. The results of this are given in Fig. 1 and show that the enthalpy change of incorporating 1 molecule of water is relatively independent of water concentration up until very large concentrations of water (∼4 wt%).

To determine the partitioning of water we used the following reactions:

$[Mg_3](Si_2, 4H)O_9 \leftrightarrow 2[2H]SiO_3 + 3[Mg]O$ Reaction 1

$[Mg](4H)O_3 + [Ca](Si)O_3$
$\qquad \leftrightarrow [Mg](Si)O_3 + [Ca](4H)O_3$ Reaction 2

$[Mg, 2H](Si_2)O_6 + [Ca](Si)O_3$
$\qquad \leftrightarrow [Mg](Si)O_3 + [Ca, 2H](Si_2)O_6$ Reaction 3

$[Mg]O + [2H]SiO_3 \leftrightarrow [2H]O + [Mg](Si)O_3$ Reaction 4

$[Mg_2, Al](Si_2, Al)O_9 + [2H](Si)O_3$
$\qquad \leftrightarrow [Mg, Al, 2H](Si_2Al)O_9 + [Mg](Si)O_3$ Reaction 5
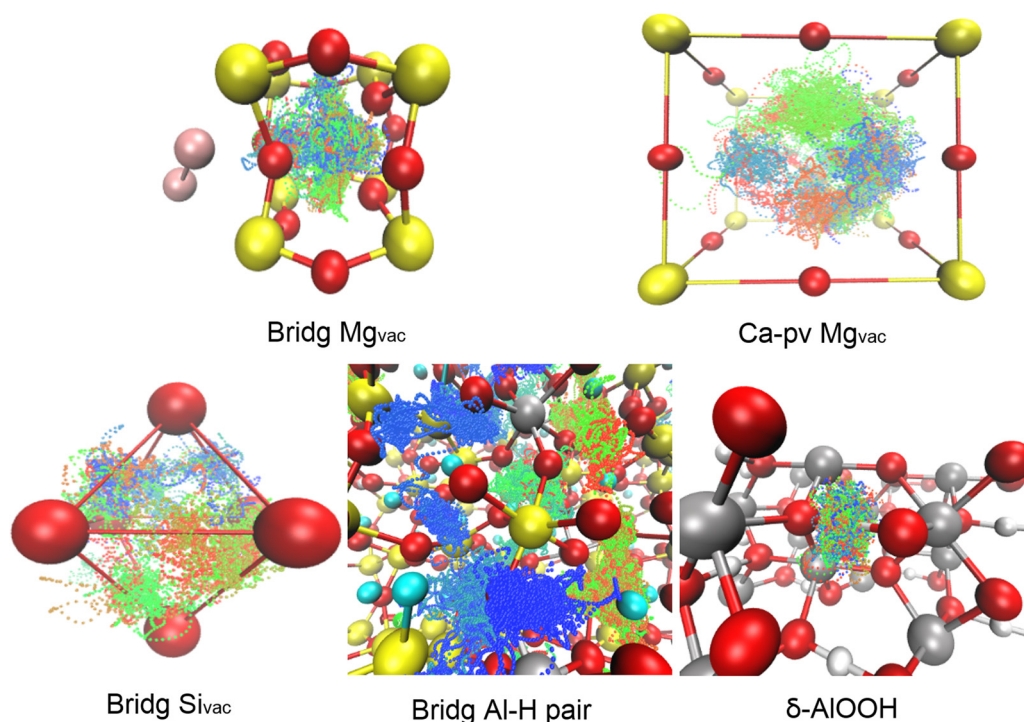
Fig. 2. Example images of the movement of a single H in different sites (a Ca vacancy in Calcium perovskite, a Mg and a Si vacancy in Bridgmanite, an Al–H pair in bridgmanite and δ-AlOOH) through time (from red = 1 ps to blue = 30 ps) at 25 GPa and 2000 K. For the Al–H pair, protons are free to move over a wide region. Similar behaviour occurs at 125 GPa and at 1000, 2000 and 3000 K. Red spheres are O, yellow spheres Si, light blue spheres Mg, grey spheres Al, white spheres H. (For interpretation of the references to colour in this figure legend, the reader is referred to the web version of this article.)

$[Mg_2, Al](Si_2, Al)O_9 + [Mg](4H)O_3$

$\leftrightarrow [Mg_2Al](Si, Al, 4H)O_9 + [Mg](Si)O_3$ Reaction 6

$[Mg, Al, 2H](Si_2, Al)O_9 + 3[Mg]O$

$\leftrightarrow [Mg_4](Si_2, AlH_2)O_{12}$ Reaction 7

$[Mg_3](Si_2, AlH_2)O_9$

$\leftrightarrow 2AlOOH + [Mg](Si)O_3 + 2[Mg]O$ Reaction 8

$[Mg_4](Si_2, AlH_2)O_{12}$

$\leftrightarrow MgSiO_4H_2 + [MgAl](Si, Al)O_6 + 2[Mg]O$ Reaction 9
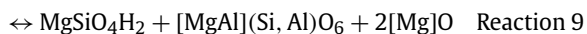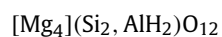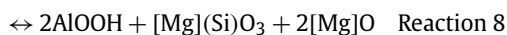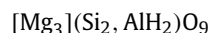
The locations of the protons are specified by denoting the A site of a ferropericlase or a perovskite-type structure with a square bracket, and those located on the B site of a perovskite-type structure with a round bracket. These reactions can be written in many different equivalent ways, but these are chosen to indicate the position of the H more clearly and to allow us to separate out the effect that Al has on bridgmanite water absorption. Actual water concentrations are much lower than represented here. A lower mantle mixture of bridgmanite:ferropericlase:Ca-pv with a ratio 75:15:10 was constructed and all partitioning reactions were carried out between those minerals in that proportion. Bridgmanite contained 5 wt% of Al_2O_3. It is assumed that the system is undersaturated in water and that a free water phase would not be formed. In all cases, the number of hydrogen atoms (as well as all other atoms) in the system is fixed. Water concentration is given as ppm by weight relative to the mantle mixture.

Free energies for reactions 1 to 9 were then determined at 25 and 125 GPa and at temperatures of 0 (static), 1000, 2000 and 3000 K from the enthalpy and the configurational entropy (as outlined in the supplementary methods). The effect of vibrational entropy is calculated in the supplementary methods and is shown to be minimal (below the statistical error of the thermal enthalpy).

After the energy of Reactions 1 to 9 was determined the partitioning of water was solved by using Equation (1):
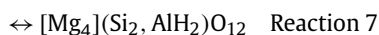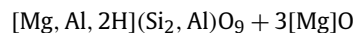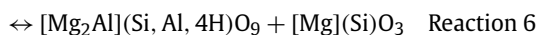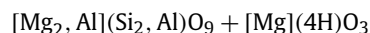
$$RT \ln K + \Delta G^0_{P,T} = 0 \tag{1}$$

where G is the standard state free energy difference of the reaction and K is the equilibrium constant for each reaction (1–9). Equation (1) was solved simultaneously for all 9 reactions using a numerical minimisation routine at the desired pressures and temperatures. The species in each equilibrium constant are listed in the supplementary methods.

Images of the hydrated vacancies are shown in Fig. 2. As can be seen, at mantle temperatures the protons are not strongly bound to a particular oxygen, but move between the different oxygens within the site. This adds a significant contribution to the configurational entropy (as discussed in the Supplementary Information). Including the within site configurational entropy is particularly important for the Al–H substitution where the protons are able to move quite far from the Al ion, and for H phases where the H are fixed to specific sites and thus have reduced configurational entropy.

3. Results

For hydrolytic weakening to be important in the lower mantle, significant water must be partitioned into a rheologically important phase—such as the volumetrically largest phase—bridgmanite—and the mechanism of incorporation must provide some sort of weakening mechanism. There are multiple sites into which water (or strictly protons) can absorb in perovskite-type structures. Water can create hydrated Mg or Ca vacancies (which are filled with 2 H^+ ions) or hydrated Si vacancies (filled with 4 H^+ ions). With the presence of Al, water can also be incorporated as an Al^{3+}–H^+ pair which replaces a Si^{4+} atom in a vacancy-free method. Water may also partition into a different phase (i.e. $CaSiO_3$ or MgO), and a dense hydrous phase may also be created (i.e. δ-AlOOH or

Table 1
Energy change of reactions 1 to 9 at 25 GPa without the configurational entropy contribution and the configurational entropy change of these reactions with 10, 100 and 1000 ppm mantle water (with 5 wt% Al_2O_3 in the Al-containing products). All reactions energies have been scaled so that they represent the transfer of 4 H atoms (2 water units) for ease of comparison.

		ΔE_{rxn} (eV/4 H)			$\Delta S config_{rxn}$ (-eV/4 HK)		
		0 K	1000 K	2000 K	10 ppm	100 ppm	1000 ppm
Al free							
	Pv-Si$_{vac}$	0.00	0.00	0.00	0.00E+00	0.00E+00	0.00E+00
R1	Pv-Mg$_{vac}$	0.57	−0.12	−0.36	−1.33E−03	−1.13E−03	−9.30E−04
R2	CaPv-Si$_{vac}$	−0.12	−1.34	−1.48	1.74E−04	1.74E−04	1.73E−04
R3	CaPv-Mg$_{vac}$	2.04	−3.30	−4.72	3.47E−04	3.47E−04	3.44E−04
R4	MgO	1.51	1.48	0.20	2.77E−04	2.77E−04	2.76E−04
Al containing							
R5	AlPv-Mg$_{vac}$	−0.97	−0.77	−1.25	8.66E−06	8.73E−06	8.81E−06
R6	AlPv-Si$_{vac}$	0.03	−0.79	−2.12	4.12E−06	4.26E−06	4.41E−06
R7	AlPv-AlH	0.47	−0.82	−1.64	−1.55E−03	−9.00E−04	−5.84E−04
R8	δ-AlOOH	−5.54	−4.48	−5.71	5.15E−03	4.04E−03	3.28E−03
R9	δ-MgSiO$_4$H$_2$	−1.84	−0.50	−1.38	4.14E−03	3.03E−03	2.25E−03

Table 2
As in Table 1, but at 125 GPa. The difference between the configurational entropy at 125 GPa and at 25 GPa is due to the energy differences included in the partition function.

		ΔE_{rxn} (eV/4 H)				$\Delta S config_{rxn}$ (-eV/4 HK)		
		0 K	1000 K	2000 K	3000 K	10 ppm	100	1000
Al free								
	Pv-Si$_{vac}$	0	0	0	0	0.00E+00	0.00E+00	0.00E+00
R1	Pv-Mg$_{vac}$	2.23	2.61	3.23	3.94	−1.37E−03	−1.17E−03	−9.69E−04
R2	CaPv-Si$_{vac}$	−0.02	0.67	0.20	−0.54	1.74E−04	1.74E−04	1.73E−04
R3	CaPv-Mg$_{vac}$	6.34	1.87	−0.58	−1.03	3.47E−04	3.47E−04	3.44E−04
R4	MgO	1.98	2.49	2.08	0.86	2.77E−04	2.77E−04	2.76E−04
Al containing								
R5	AlPv-Mg$_{vac}$	1.04	−0.92	−1.70	−1.33	8.66E−06	8.70E−06	8.80E−06
R6	AlPv-Si$_{vac}$	0.58	1.47	0.86	0.00	4.85E−06	4.64E−06	4.46E−06
R7	AlPv-AlH	−0.88	1.51	2.03	0.87	−1.53E−03	−9.05E−04	−8.20E−04
R8	δ-AlOOH	−5.61	−7.39	−7.64	−7.09	5.14E−03	4.09E−03	3.54E−03
R9	δ-MgSiO$_4$H$_2$	−2.53	−3.81	−3.40	−1.86	4.13E−03	3.07E−03	2.50E−03

$MgSiO_4H_2$) (Sano et al., 2008; Tsuchiya, 2013; Ohira et al., 2014; Walter et al., 2015). Of those, only the creation of Mg or Si vacancies is likely to affect the rheology of the mantle.

The energies and entropies of Reactions 1–9 are given in Tables 1–2. From these the partitioning of water among all possible sites and phases was calculated at various conditions and water concentrations. Fig. 3 shows the concentration of water in various sites in the different phases along a lower mantle geotherm for three different concentrations of total water. The results show that the amount of water in each phase varies strongly with depth and also varies strongly with total water content. For instance, if the total water content is low (100 ppm) then the water is preferentially incorporated into bridgmanite as Al–H pairs throughout the lower mantle. For 1000 ppm of total water, Ca-pv becomes the dominant host at the top of the lower mantle until about 1000 km depth where the AlH pair in bridgmanite becomes more favoured. For very high concentrations of water (∼5000 ppm) the depth range where Ca-pv is the main host for water is extended to about 1200 km. Changes in the distribution in water between the phases can be understood in the normal way as a balance between volumetric and entropic effects on the free energy. The formation of AlH pairs is strongly favoured by configurational entropy and this effect is dominant at lower water concentrations. With increasing water the formation of Ca vacancies becomes more favoured due to volumetric effects becoming more important and configurational entropy becoming less important, but AlH pairs remain dominant throughout most of the lower mantle for all concentrations tested.

It should be noted that we have calculated the equilibrium partitioning assuming a given amount of water in the mineral phases and not the absolute solubility. However, even if the system is wa-
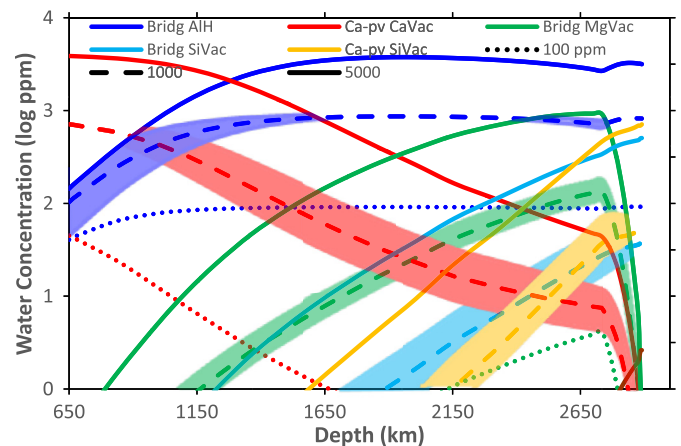

Fig. 3. Distribution of total water amongst the various possible sites along the geotherm of Ono (2008). The results are shown for 100, 1000 and 5000 ppm water (defined against a mantle mixture of Al-pv:fp:ca-pv of 75:15:10). Ferropericlase adsorbs less than 1 ppm water under all these conditions and δ-AlOOH or MgSiO$_4$H$_2$ are not produced with this amount of water and ferropericlase. For the 1000 ppm curves the shading represents statistical error—the energy of each system was determined to within 1.5 eV/atom and the error in the concentration of water was calculated independently by propagating this error throughout all the reactions.

ter saturated, the relative concentrations in the different phases will be the same as the relative concentrations shown in Fig. 3. For instance, if the system becomes saturated such that there is a total water content of 1000 ppm distributed in the mineral phases, then most of that water will be in Ca-pv until about 1000 km depth,

when it then partitions into bridgmanite as shown in Fig. 3. Alternatively, if the solubility of water in mantle phases is much lower (i.e. 100 ppm), then most of it will be in bridgmanite through the whole of the lower mantle.

Our results also show that neither δ-AlOOH nor MgSiO$_4$H$_2$ are produced in the lower mantle at low concentrations of water. At <1000 ppm water, both phases react with MgO and dissolve into bridgmanite due to the strong entropy of mixing. At lower mantle temperatures around 6000 ppm water is needed to form δ-AlOOH. We have not, however, considered the possibility of a solid solution between δ-AlOOH and MgSiO$_4$H$_2$ in this analysis which may increase the stability of these phases. This would have the effect of lowering the amount of water in all the other phases.. Similarly we have not considered the effect of stishovite as in Panero et al. (2014). In that study they argue that bridgmanite remains dry since AlH prefers to be incorporated into stishovite over bridgmanite. If true this would also lower the amount of water in the other phases, and as discussed below, reduces further the number of vacancies available for hydrolytic weakening.

We also find that periclase remains practically dry in the lower mantle. This is in agreement with the DFT calculations of Hernandez et al. (2013) on Al-free perovskite who also found a strong preference of water into bridgmanite. However, the agreement is not quite as good as it seems, since in Al-free bridgmanite and at low pressures (<∼25 GPa at 2000 K) we find that there is a much milder preference for placing water in bridgmanite. The difference can be attributed to the lack of thermal enthalpy in the study of Hernandez et al. (2013) since our static results are very similar and also predict a strong partitioning of water into Al-free bridgmanite if thermal enthalpy is ignored (see reaction 4 in Table 1). Dry periclase is also predicted by Merli et al. (2016) using hybrid-DFT and lattice dynamics, although they do not predict such an extreme partitioning as us. Some of the difference may be their use of lattice dynamics which will not fully capture the free movement of H in an AlH pair. With increasing pressure, water prefers bridgmanite to periclase in both Al-free and Al-bearing systems.

Our results show that for small amounts of water (few hundred ppm) most of the water is partitioned into Al-bearing bridgmanite, however, it is incorporated as Al–H pairs which does not increase the number of Mg or Si vacancies. As such most of the water incorporated into bridgmanite will not increase Si or Mg diffusion rates and so is unlikely to contribute to hydrolytic weakening. However, a small amount of the available water is incorporated into Si and Mg vacancies as (4 H)$_{Si}$ and (2 H)$_{Mg}$ respectively, and these may contribute to enhancing diffusion rates of Si and Mg and to hydrolytic weakening. These are shown in Fig. 4 for 10, 100 and 1000 ppm total water. At low concentrations (10 ppm) the number of Mg and Si vacancies created by water is below 0.1 ppm throughout the mantle. At higher concentrations of water, a significant number of Mg vacancies is produced, reaching 100 ppm for 1000 ppm water. On the other hand, the concentration of hydrated Si vacancies is extremely low at all water concentrations. For 100 ppm water the number of Si vacancies ranges from parts per trillion to only 0.1 ppm at about 2500 km depth. The number of Si vacancies only exceeds 10 ppm when there is 1000 ppm water, and even then only in the very deepest part of the mantle.

Also shown in Fig. 4 is the number of vacancies in perovskite required for diffusion creep in the mantle (Ammann et al., 2010; Glišović et al., 2015). Since the diffusion rates of Mg and Si vacancies in bridgmanite are similar (Ammann et al., 2010; Xu et al., 2011) and ∼2 orders of magnitude slower than O (Dobson et al., 2008), the concentration of both Si and Mg vacancies must be increased by water in order to produce hydrolytic weakening as they are both rate-limiting. As can be seen in Fig. 4, only Mg vacancies are increased by an amount that could exceed the number required
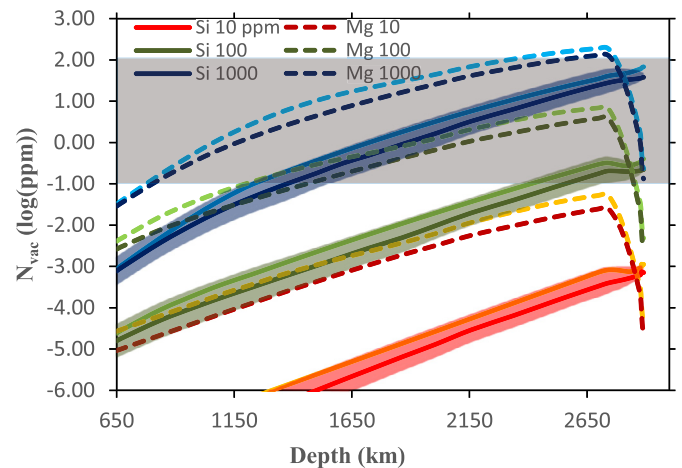

Fig. 4. Plot of the absolute amount of either Si or Mg vacancies in bridgmanite (in ppm by wt) as a function of depth (along the geotherm of Ono, 2008) and with varying total water content. The shading represents the statistical error as in Fig. 3. The grey horizontal bar at the top is the expected amount of vacancies in bridgmanite required to explain diffusion creep in the lower mantle. A lighter colour line above each line represents the effect of adding 5% iron with an Fe^{3+}/Fe^{total} ratio of 0.8 as described in the Supplementary methods.

for diffusion creep. On the other hand, the number of Si vacancies produced by water is much lower. Only if the water content is high (1000 ppm) does the concentration of hydrated vacancies become high enough to affect diffusion creep, and even then only if the grain size of the mantle is 0.1 mm or less and then only below 1250 km. At ∼100 ppm, the number of Si vacancies only becomes significant for diffusion creep at the very base of the lower mantle (>2500 km), but again only if the mantle grain size is very small. In other words, throughout the bulk of the mantle, and for reasonable water contents (∼100 ppm), water has an insignificant effect on the number of Si vacancies.

A complicating factor in the mantle is the presence of both ferrous and ferric iron in bridgmanite. Ferrous iron can replace Mg^{2+} cations and should have only minor effects on the stability of the major hydrous products as Fe^{2+} and Mg^{2+} are expected to have similar effects on nearby vacancies and H$^+$ atoms. Ferrous iron, however, can transform to ferric iron and iron metal which converts Al^{3+}–Al^{3+} pairs into Fe^{3+}–Al^{3+} pairs and so reduces the amount of Al^{3+} available to form AlH complexes. The expected magnitude of this effect is plotted in Fig. 4 and is very minor.

4. Discussion

Our results show that most water in bridgmanite is incorporated via Al–H pairs and that water only increases the concentration of Si vacancies by a trivial amount. Due to its small grain size (Solomatov et al., 2002; Solomatov and Reese, 2008) and the lack of any significant anisotropy throughout most of the lower mantle (e.g. Karato, 1998), it is generally assumed that bridgmanite deforms by diffusion creep and so our results suggest that water would not produce hydrolytic weakening in bridgmanite. While texture development indicative of dislocation creep has been seen in some bridgmanite deformation experiments (see for example Miyagi and Wenk, 2016 and the references contained within), other studies have shown no texture development (Merkel et al., 2003; Miyajima et al., 2009). Recently Tsujino et al. (2016) produced texture in bridgmanite, but only at very high strain rates (10^{-4} s^{-1}) and high stresses. Nevertheless, even if the mantle does deform via dislocation creep, deformation simulations show that while dislocation glide is the favoured deformation mechanism at low temperatures and high strain rates, the stresses for glide become too large at high pressure and some

sort of diffusion controlled mechanism is the dominant mechanism under the conditions of the lower mantle (Hirel et al., 2016b; Kraych et al., 2016). A recent suggestion is that the mantle may deform via pure dislocation climb, but this mechanism is also diffusion mediated and requires similar concentrations of vacancies as diffusion creep (Hirel et al., 2016a). Regardless of the exact mechanism, the rate determining step in both dislocation climb, climb mediated dislocation creep and diffusion creep is diffusion of the slowest atomic species. In bridgmanite this is both Si and Mg and the diffusion of these species depends on both the mobility and the concentration of the cation vacancies. As shown here, water has only a small effect on the concentration of the rate limiting vacancies and so a vacancy-concentration mechanism of hydrolytic weakening cannot occur.

While increasing vacancy concentration is the most widely cited method for hydrolytic weakening (Karato et al., 1986; Mei and Kohlstedt, 2000a; Karato and Jung, 2003; Faul et al., 2016), there are alternative mechanisms to consider. For instance, the rate of diffusion depends not only upon the concentration of vacancies, but also on their mobility. It is possible that hydration of the vacancies in bridgmanite increases their mobility by lowering the migration barrier to jump. Although this has not been measured in bridgmanite, in chemically similar olivine the activation energies of Fe–Mg interdiffusion (Kohlstedt and Mackwell, 2008) and Si (Fei and Katsura, 2016; Fei et al., 2016) diffusion in wet and dry systems are the same and only vacancy concentration is important in explaining the increased diffusion rates in water-bearing olivine. This is an important avenue for future research however.

It is also possible that hydrolytic weakening occurs via weakening of grain boundaries or by strongly enhancing grain boundary diffusion. While we cannot rule these out from our results, Coble creep or grain boundary sliding mechanisms are normally the active deformation mechanism only for small grain sizes. Unfortunately the grain size of the lower mantle is currently unknown and so its deformation map remains uncertain. However, in perovskite, Si bulk diffusion is dominant over grain boundary diffusion except when the grain size is <10 μm (Nishi et al., 2013). So unless the grain size of the lower mantle is exceedingly small, deformation is likely to be via diffusion creep rather than grain boundary diffusion creep. Nevertheless, our results do not rule out water weakening of grain boundaries and requires further work.

It is has been suggested that hydrolytic weakening in olivine is associated with the incorporation of Ti^{4+} (Faul et al., 2016). In olivine Ti^{4+} can substitute for Mg^{2+} which is charge balanced by two protons in the Si site. This increases the number of Si vacancies available for diffusion and provides a weakening mechanism. This mechanism, however, is unlikely to occur in the lower mantle due to the fact that Ti readily substitutes into octahedral sites in many silicates and oxides (Berry et al., 2007). While in olivine, Mg^{2+} is located in an octahedral site and Si is located in a tetrahedral site, in perovskite structures Si is located in an octahedral site while Mg is located in a higher-coordinated site. Therefore the number of Ti^{4+} ions replacing Mg^{2+} in bridgmanite is expected to be significantly lower than in olivine. Indeed the original perovskite is $CaTiO_3$ which makes a full solid solution with $CaSiO_3$. Full verification of this will, however, require further work.

Finally there is some discussion as to the phase that controls deformation in the lower mantle with two recent studies (Girard et al., 2016; Kaercher et al., 2016) suggesting that the volumetrically smaller and weaker phase, ferropericlase, may control deformation rather than the larger, stronger phase bridgmanite. If ferropericlase does indeed control deformation in the lower mantle then water should have negligible effects on lower mantle rheology since our results show that ferropericlase remains essentially dry throughout the lower mantle.

In conclusion our results suggest that water will not have a significant effect on mantle rheology. This is in direct contrast to the generally held view that water strongly affects the rheology of the mantle as a whole. Our results suggest that water can therefore be considered as a passive component in the lower mantle and is not expected to have a strong effect on lower mantle dynamics.

Acknowledgements

Appendix A. Supplementary material

Supplementary material related to this article can be found online at https://doi.org/10.1016/j.epsl.2017.11.051.

References

Ammann, M.W., Brodholt, J.P., Wookey, J., Dobson, D.P., 2010. First-principles constraints on diffusion in lower-mantle minerals and a weak D″ layer. Nature 465, 462–465.

Berry, A.J., Walker, A.M., Hermann, J., O'Neill, H.S., Foran, G.J., Gale, J.D., 2007. Titanium substitution mechanisms in forsterite. Chem. Geol. 242, 176–186.

Crowley, J.W., Gerault, M., O'Connell, R.J., 2011. On the relative influence of heat and water transport on planetary dynamics. Earth Planet. Sci. Lett. 310, 380–388.

Dobson, D.P., Dohmen, R., Wiedenbeck, M., 2008. Self-diffusion of oxygen and silicon in MgSiO_3 perovskite. Earth Planet. Sci. Lett. 270, 125–129.

Faul, U.H., Cline, C.J., David, E.C., Berry, A.J., Jackson, I., 2016. Titanium-hydroxyl defect-controlled rheology of the Earth's upper mantle. Earth Planet. Sci. Lett. 452, 227–237.

Fei, H.Z., Katsura, T., 2016. Si and O self-diffusion in hydrous forsterite and iron-bearing olivine from the perspective of defect chemistry. Phys. Chem. Miner. 43, 119–126.

Fei, H.Z., Koizumi, S., Sakamoto, N., Hashiguchi, M., Yurimoto, H., Marquardt, K., Miyajima, N., Yamazaki, D., Katsura, T., 2016. New constraints on upper mantle creep mechanism inferred from silicon grain-boundary diffusion rates. Earth Planet. Sci. Lett. 433, 350–359.

Fei, H.Z., Wiedenbeck, M., Yamazaki, D., Katsura, T., 2013. Small effect of water on upper-mantle rheology based on silicon self-diffusion coefficients. Nature 498, 213–215.

Girard, J., Amulele, G., Farla, R., Mohiuddin, A., Karato, S., 2016. Shear deformation of bridgmanite and magnesiowüstite aggregates at lower mantle conditions. Science 351, 144–147.

Glišović, P., Forte, A.M., Ammann, M., 2015. Variations in grain size and viscosity based on vacancy diffusion in minerals, seismic tomography, and geodynamically inferred mantle rheology. Geophys. Res. Lett. 42, 6278–6286.

Griggs, D.T., Blacic, J.D., 1965. Quartz – anomalous weakness of synthetic crystals. Science 147, 292–295.

Grimme, S., Antony, J., Ehrlich, S., Krieg, S., 2010. A consistent and accurate ab initio parametrization of density functional dispersion correction (DFT-D) for the 94 elements H–Pu. J. Chem. Phys. 132, 154101.

Hernandez, E., Alfe, D., Brodholt, J., 2013. The incorporation of water into lower-mantle perovskites: a first-principles study. Earth Planet. Sci. Lett. 364, 37–43.

Hirel, P., Carrez, P., Clouet, E., Cordier, P., 2016a. The electric charge and climb of edge dislocations in perovskite oxides: the case of high-pressure MgSiO_3 bridgmanite. Acta Mater. 106, 313–321.

Hirel, P., Carrez, P., Cordier, P., 2016b. From glissile to sessile: effect of temperature on ⟨110⟩ dislocations in perovskite materials. Scr. Mater. 120, 67–70.

Honing, D., Spohn, T., 2016. Continental growth and mantle hydration as intertwined feedback cycles in the thermal evolution of Earth. Phys. Earth Planet. Inter. 255, 27–49.

Kaercher, P., Miyagi, L., Kanitpanyacharoen, W., Zepeda-Alarcon, E., Wang, Y., Parkinson, D., Lebensohn, R.A., De Carlo, F., Wenk, H.R., 2016. Two-phase deformation of lower mantle mineral analogs. Earth Planet. Sci. Lett. 456, 134–145.

Karato, S.I., 1998. Seismic anisotropy in the deep mantle, boundary layers and the geometry of mantle convection. Pure Appl. Geophys. 151, 565–587.

Karato, S.I., Jung, H., 2003. Effects of pressure on high-temperature dislocation creep in olivine. Philos. Mag. 83, 401–414.

Karato, S.I., Paterson, M.S., Fitz Gerald, J.D., 1986. Rheology of synthetic olivine aggregates – influence of grain-size and water. J. Geophys. Res., Solid Earth Planets 91, 8151–8176.

Kohlstedt, D., 2006. The role of water in high-temperature rock deformation. Rev. Mineral. Geochem. 62, 377–396.

Kohlstedt, D., Mackwell, S., 2008. The role of protons in ionic diffusion in $(Mg,Fe)O$ and $(MgFe)_2SiO_4$. J. Mater. Sci. 43, 4693–4700.

Korenaga, J., 2011. Thermal evolution with a hydrating mantle and the initiation of plate tectonics in the early Earth. J. Geophys. Res., Solid Earth 116, B124031.

Kraych, A., Carrez, P., Cordier, P., 2016. On dislocation glide in $MgSiO_3$ bridgmanite at high-pressure and high-temperature. Earth Planet. Sci. Lett. 452, 60–68.

Kresse, G., Furthmuller, J., 1996. Efficient iterative schemes for ab-initio total-energy calculations using a plane-wave basis set. Phys. Rev. B 54, 11169–11186.

Kresse, G., Joubert, D., 1999. From ultrasoft pseudopotentials to the projector augmented-wave method. Phys. Rev. B 59, 1758.

Mei, S., Kohlstedt, D.L., 2000a. Influence of water on plastic deformation of olivine aggregates 1. Diffusion creep regime. J. Geophys. Res., Solid Earth 105, 21457–21469.

Mei, S., Kohlstedt, D.L., 2000b. Influence of water on plastic deformation of olivine aggregates 2. Dislocation creep regime. J. Geophys. Res., Solid Earth 105, 21471–21481.

Merkel, S., Wenk, H.R., Badro, J., Montagnac, G., Gillet, P., Mao, H.K., Hemley, R.J., 2003. Deformation of $(Mg_{0.9},Fe_{0.1})SiO_3$ perovskite aggregates up to 32 GPa. Earth Planet. Sci. Lett. 209, 351–360.

Merli, M., Bonadiman, C., Diella, V., Pavese, A., 2016. Lower mantle hydrogen partitioning between periclase and perovskite: a quantum chemical modelling. Geochim. Cosmochim. Acta 173, 304–318.

Miyagi, L., Wenk, H.R., 2016. Texture development and slip systems in bridgmanite and bridgmanite + ferropericlase aggregates. Phys. Chem. Miner. 43, 597–613.

Miyajima, N., Yagi, T., Ichihara, M., 2009. Dislocation microstructures of $MgSiO_3$ perovskite at a high pressure and temperature condition. Phys. Earth Planet. Inter. 174, 153–158.

Nakagawa, T., Nakakuki, T., Iwamori, H., 2015. Water circulation and global mantle dynamics: insight from numerical modeling. Geochem. Geophys. Geosyst. 16, 1449–1464.

Nishi, M., Nishihara, Y., Irifune, T., 2013. Growth kinetics of $MgSiO_3$ perovskite reaction rim between stishovite and periclase up to 50 GPa and its implication for grain boundary diffusivity in the lower mantle. Earth Planet. Sci. Lett. 377–378, 191–198.

Nose, S., 1984. A molecular-dynamics method for simulations in the canonical ensemble. Mol. Phys. 52, 255–268.

Ohira, I., Ohtani, E., Sakai, T., Miyahara, M., Hirao, N., Ohishi, Y., Nishijima, M., 2014. Stability of a hydrous δ-phase, $AlOOH$–$MgSiO_2(OH)_2$, and a mechanism for water transport into the base of lower mantle. Earth Planet. Sci. Lett. 401, 12–17.

Ono, S., 2008. Experimental constraints on the temperature profile in the lower mantle. Phys. Earth Planet. Inter. 170, 267–273.

Panero, W.R., Pigott, J.S., Reaman, D.M., Kabbes, J.E., Liu, Z., 2014. Dry $(Mg,Fe)SiO_3$ perovskite in the Earth's lower mantle. J. Geophys. Res. 120, 894–908.

Perdew, J.P., Ruzsinszky, A., Csonka, G.I., Vydrov, O.A., Scuseria, G.E., Constantin, L.A., Zhou, X.L., Burke, K., 2008. Restoring the density-gradient expansion for exchange in solids and surfaces. Phys. Rev. Lett. 100, 1364061. 4 pp.

Sandu, C., Lenardic, A., McGovern, P., 2011. The effects of deep water cycling on planetary thermal evolution. J. Geophys. Res., Solid Earth 116, B124041. 15 pp.

Sano, A., Ohtani, E., Kondo, T., Hirao, N., Sakai, T., Sata, N., Ohishi, Y., Kikegawa, T., 2008. Aluminous hydrous mineral δ-$AlOOH$ as a carrier of hydrogen into the core-mantle boundary. Geophys. Res. Lett. 35, L033031. 5 pp.

Solomatov, V.S., El-Khozondar, R., Tikare, V., 2002. Grain size in the lower mantle: constraints from numerical modeling of grain growth in two-phase systems. Phys. Earth Planet. Inter. 129, 265–282.

Solomatov, V.S., Reese, C.C., 2008. Grain size variations in the Earth's mantle and the evolution of primordial chemical heterogeneities. J. Geophys. Res., Solid Earth 113, B074081. 21 pp.

Tkatchenko, A., Scheffler, M., 2009. Accurate molecular Van Der Waals interactions from ground-state electron density and free-atom reference data. Phys. Rev. Lett. 102, 0730051. 4 pp.

Tsuchiya, J., 2013. First principles prediction of a new high-pressure phase of dense hydrous magnesium silicates in the lower mantle. Geophys. Res. Lett. 40, 4570–4573.

Tsujino, N., Nishihara, Y., Yamazaki, D., Seto, Y., Higo, Y., Takahashi, E., 2016. Mantle dynamics inferred from the crystallographic preferred orientation of bridgmanite. Nature, 81–85.

Walter, M.J., Thomson, A.R., Wang, W., Lord, O.T., Ross, J., McMahon, S.C., Baron, M.A., Melekhova, E., Kleppe, A.K., Kohn, S.C., 2015. The stability of hydrous silicates in Earth's lower mantle: experimental constraints from the systems MgO–SiO_2–H_2O and MgO–Al_2O_3–SiO_2–H_2O. Chem. Geol. 418, 16–29.

Xu, J., Yamazaki, D., Katsura, T., Wu, X., Remmert, P., Yurimoto, H., Chakraborty, S., 2011. Silicon and magnesium diffusion in a single crystal of $MgSiO_3$ perovskite. J. Geophys. Res. 116, B122051. 8 pp.